Paper III

Production of ATLAS silicon detector modules - Report from the Scandinavian Cluster

Lars G. Johansen*, Bjarte Mohn*, Arne Solberg*, Bjarne Stugu*,
Ola Kristoffer Øye*, Ole Dorholt†, Torkjell Huse†, Steinar Stapnes †,
Nils Bingefors‡, Richard Brenner‡, Stefan Ehn‡, Tord Ekelöf‡,
Lars Eklund‡, Lars-Erik Lindquist‡

May, 2006

ATL-INDET-PUB-2006-003
12 June 2006

Abstract

This document describes the assembly and quality assurance of Semi Conductor Tracker (SCT) barrel modules performed by the Scandinavian Cluster. The project has been carried out as a joint effort between University of Bergen, University of Oslo and Uppsala University.

1 Introduction

Constructing the ATLAS detector for CERN's Large Hadron Collider (LHC) is a huge effort that involves about 1500 physicists and a similar number of engineers and technicians from more than 150 institutions from all over the world. While some construction tasks are prohibitively large, a very large fraction of the tasks is modular in its nature, permitting smaller groups to take on significant responsibilities. The ATLAS SCT (Semi Conductor Tracker) detector system [1] is an excellent example of such a modular system. For the barrel part of the system (defining roughly half of the SCT), 10650 silicon detectors were to be used for the assembly of 2600 detector modules of which 2112 were to be mounted and used in the detector system. The surplus modules are for spares and to allow for failures in the production process.

Given long standing involvements in silicon systems and silicon detector development in Norway and Sweden, the SCT was a natural place to channel resources. Moreover Uppsala, Oslo and Bergen decided to join forces in an effort to deliver detector modules for the barrel part of the SCT. The production of these modules is now successfully completed, and the purpose of this document is to describe the production process, which covers the testing of individual components, the assembly of the components to working modules and finally the testing and classification of the modules delivered.

*Department of Physics and Technology, University of Bergen
†Department of Physics, University of Oslo
‡Department of Radiation Sciences, Uppsala University

2 Sensor-baseboard Assembly

The assembly of four silicon strip sensors on a baseboard was done at the University of Oslo. A double sided module was made by glueing two sensors on each side of the TPG baseboard. The two sensors on each side were aligned such that the strips can be bonded together to give 120 millimeters long strips. The front-side sensors must be aligned relative to the back-side sensors with a precision of five micrometers, and the sensors relative to the baseboard with a precision of 30 micrometers. In this section a description of the glueing and aligment procedures is given. A brief description of the geometrical parameters defining the tolerances is given in the section 3.

2.1 Jigs and Tooling

The first step in the assembly procedure was to align two sensors relative to each other. This was done with an alignment station consisting of two positioning units with a vacuum chuck, two linear stages and a rotating stage [1] , mounted on a solid aluminium base plate. Aluminium blocks with inserts of press fitted line bearings, for guiding the pick-up jigs when transfering the aligned sensors away from the alignment station, [2] are attached to the base plate on both sides of the positioning stages. The alignment station is compact to make the lever arm between the linear bearings as short as possible, which is crucial for minimizing induced misalignment when the sensors are transfered from the positioning stages to the pick-up jig. Fiducial marks have been glued on top of the aluminium blocks, which are used as references in the alignment procedure. The alignment station is mounted on two long range linear stages driving it under the microscope that is kept in a fixed position. The sensor have fiducial markes processed on the surface allowing optical alignment with a pattern recognition software. The system of microscop, pattern recognition and operation of step-motors are controlled by a LabVIEW program that ensured stability and repeatability in the process. The alignment station with two sensors is shown in figure 1.

Two pairs of sensors were aligned and placed on pick-up jigs before final assembly into a sensor-baseboard sandwich. These pick-up jigs also served as assembly jigs. The jig holding the sensors for the back-side of the module has steering pins for the positioning of the baseboard. The pick-up jigs have line bearings of the same type as in the aluminium block of the alignment station. Two round bars that have been precisely matched with the jig line bearings guide and align the two pick-up jigs in the assembly procedure. A jig-set is shown in figure 2.

The jigs hold the sensors and baseboards with vacuum. Grooves have been machined into the jigs to spread the vacuum over the sensor surface. Clean room paper was put between the sensor and the jig to protect the surface from scratches or other damage. It was found that is the holes in the baseboards had a slight variation in diameter. To achive the required precision the steering pins had to fit tightly in the holes, and replacable pins with four different diameters were made for the jig. The positions of the steering pins are fixed, so the backside sensors must be aligned relative to these pins. The position of the front side jig on the back side jig is also fixed by the round bar through the linear bearings. Hence, the front side sensors had to be aligned after the back-side sensors.

[1] NEPLES COOBE Ltd, UK, Model: BERGER-LAHR RDM 543/100LTA
[2] STAR LiniærTeknikk AS, Norway, model: 0658-22-30

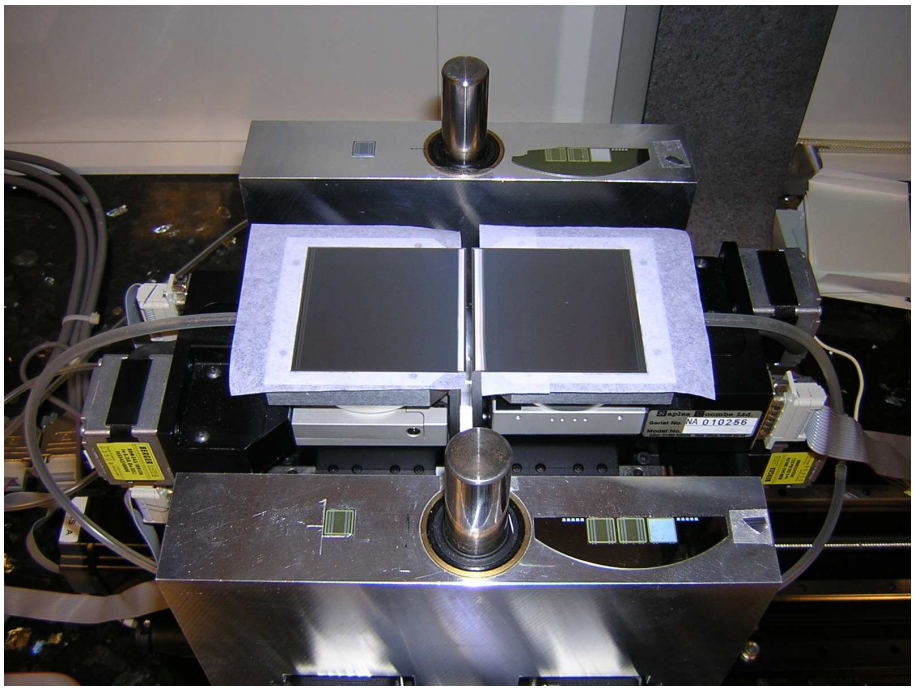

Figure 1: *The alignment station used for the alignment of two sensors. Each sensor is controlled by two linear stages and a rotating stage, and is aligned relative to fiducials on the aluminum frame.*

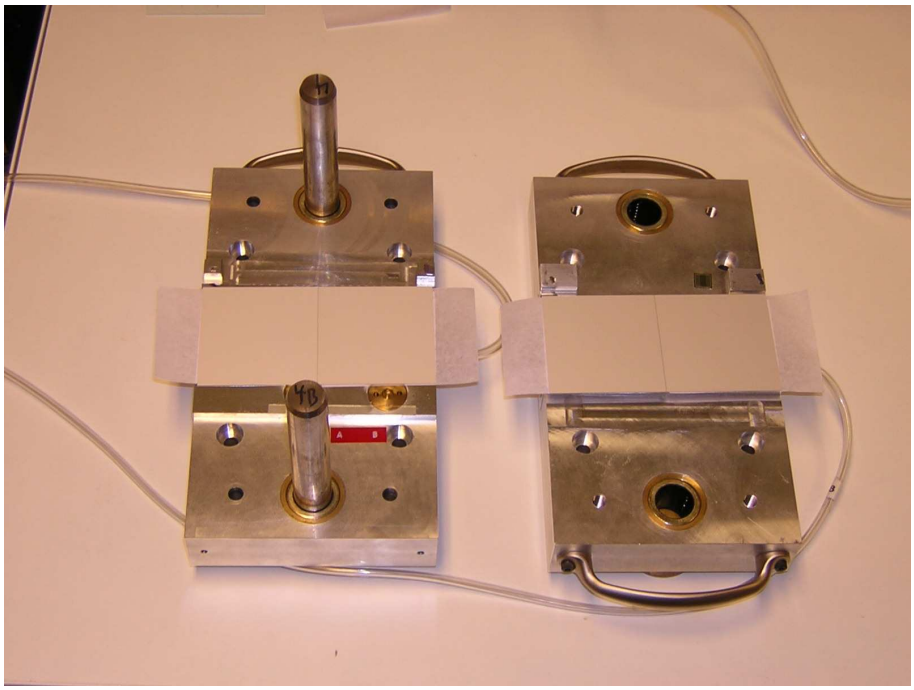

Figure 2: *Two pick-up jigs make up a jig set. The backside jig has steering pins for the baseboard.*

A glue dispenser robot [3] was used to apply the adhesive on the baseboard. The dispenser head was controlled by air pressure, and could control the amount of glue in dots or continuous lines. The head was controlled by three linear stages; in the x- and y-direction to define the pattern, and in z to give the correct height of the surface.

2.2 Alignment of Sensors

Two sensors making up one side of the module were aligned on the alignment station. The position of a sensor is defined by fiducial marks on the surface. The fiducials on the alignment frame were measured first, and then the positions of the sensors were calculated depending on which pick-up jig that was used. The alignment procedure was an iterative process were the fiducials on the sensors were measured and compared to the target positions. If the deviations were bigger than 1.5 micrometer from nominal value, the sensors were rotated and shifted to hit the target positions, and re-measured.

After the alignment of the sensors they were transfered to the pick-up jig by sliding the jig down using the round bar in the linear bearings on the alignment frame. When the jig was resting on the sensor surfaces, the vacuum was switched from the vacuum chucks on the positioning units to the pick-up jig.

The quality of the transfer from the alignment system to the pick-up jigs was cross-checked by measuring the sensors positions relative to two reference points on the jig. Since the sensors were on the pick-up jigs with the backside facing up, the fiducial marks could no longer be used. Instead, the corners of the sensors were used to define the sensor positions in these measurements. The location of the corners relative to the fiducial marks were precisely calculated in the alignment station to eliminate the errors from cut-edge variations.

If the sensors had moved by more than three micrometers during the transfer from the alignment system to the pick-up jig the alignment pocedure had to be repeated.

2.3 Assembly of the Sensors to the Baseboard

When both the backside and front-side sensors had been successfully aligned and transfered to the pick-up jigs, they were glued to the baseboard. Two types of adhesives were used; 2011 two-component Araldite mixed with boron nitrite for high thermal conductivity, and a silver epoxy to give electrical contact between the baseboard and the backplane of the sensor. The glue robot was used to apply the Araldite to the baseboard in the specified pattern on both sides. The silver epoxy was applied by hand on the eight contact points on the baseboard.

The back-side pick-up jig had two steering pins fitted for the hole and slot on the baseboard facing. This provided the required precision of 30 micrometers in the x- and y-direction of the positioning of the baseboard. To keep the baseboard in plane with the sensors, and also to control the glue thickness, spacers were put on both sides of the small facing of the baseboard to fix the gap between the facing and the jig surface. Using the round bar the front-side jig was lowered down on the back-side jig, bringing the front-side sensors down on the baseboard. The front-side jig would rest on the spacer put on top of the baseboard facing. To control the total thickness of the module, a spacer was put

[3] Martin Auto Dispenser DotLinear04

between the two jigs. Finally, the module was left for about 24 hours to allow for the glue to cure.

3 Metrology

One of the goals of the production was to reach an assembly precision of silicon detector modules significantly better than their position resolution of 22μm in $R\phi$ and 580μm in Rz. If the assembly error is negligible to the position resolution all produced modules can be treated in the alignment algorithm as identical. The impact of misalignment in the ATLAS Inner Detector have been studied by simulating tracks with P_T between 4 and 500 GeV [2], and the alignment tolerances in the xy-plane were derived from this study. The out-of-plane tolerances are driven by the separation of the surfaces of adjacent silicon detector modules. The silicon sensors in the detector modules have an intrinsic bow, figure 3, which make the sensor deviate from a perfect flat plane. All detector modules have the same built in bow which is defined as a common profile. The common profiled used in Scandinavia was compiled from a set of modules produced at KEK, Japan.

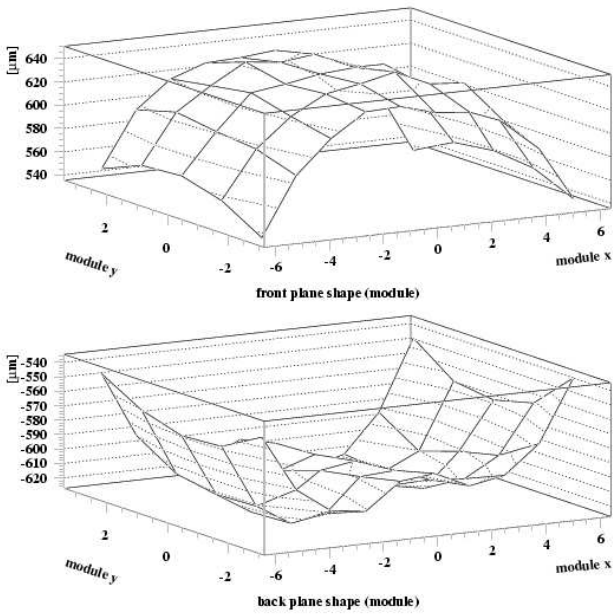

Figure 3: The upper and the lower figures show the bowing on the upper and the lower surfaces of detector modules. The y-axis is given in absolute coordinates with the central plane of the detector module defined as reference.

3.1 Alignment parameters

An original set of alignment tolerances is given in the SCT Final Design Review documentation [3]. The document specifies 13 alignment tolerances in xy-plane and 2 out-of-plane tolerances. In addition to this set of parameters additional parameters were defined in

order to control the quality at the production sites. The full set of alignment parameters are 21 in xy-plane and 26 in out-of-plane. The extra parameters in xy-plane define the position of the hybrid. In out-of-plane, the extra parameters make a more detailed characterization of the shape of silicon sensors and the out-of-plane dimensions of the hybrid. Most assembly tolerances were generous and easily met by the assembly procedure. A few tolerances were tight and had to be given special care to be met. The tight parameters were the alignment of the upper and lower silicon sensors in the direction transverse to the strips (midyf) with an assembly tolerance of 5μm, the individual angles of each sensor (a1-a4) with an assembly tolerance of 0.13 mrad and the stereo angle (stereo) between silicon strips on the upper and lower silicon planes with an assembly tolerance of 0.13 mrad. In the start of the production the assembly tolerances of the hybrid were not achieved, the reason being that the tolerances for the hybrid were specified after the hybrid assembly fixtures and procedures were designed. Once the tolerances were approved new jigs and procedures were designed bringing the hybrid assembly inside tolerances. In out-of-plane the parameters that were most critical were the deviation of the module shape from the common profile (optimalMaxZerrorLower, optimalMaxZerrorUpper) with an assembly precision of 50 μm and the transverse bowing of the module facings (loCoolingFacing b) along y-axis with an assembly tolerance of 3 mrad.

3.1.1 Measurement procedure

The detector module survey was done in a class 100000 clean room, controlled to a temperature of 21°C +/- 1°C, with a Smartscope Flare Flash1 optical measurement machine [4]. The machine measures a volume of $200x200x150mm^3$. The resolution on XYZ axis' is 0.5 μm and the absolute measurement accuracy is $(2.5 + 5L/1000)\mu$m in XY-plane and $(3 + 6L/1000)\mu$m in Z, where L is the measuring length given in mm. The modules were measured with 560X magnification. The measurement machine with operator is shown in figure 4.

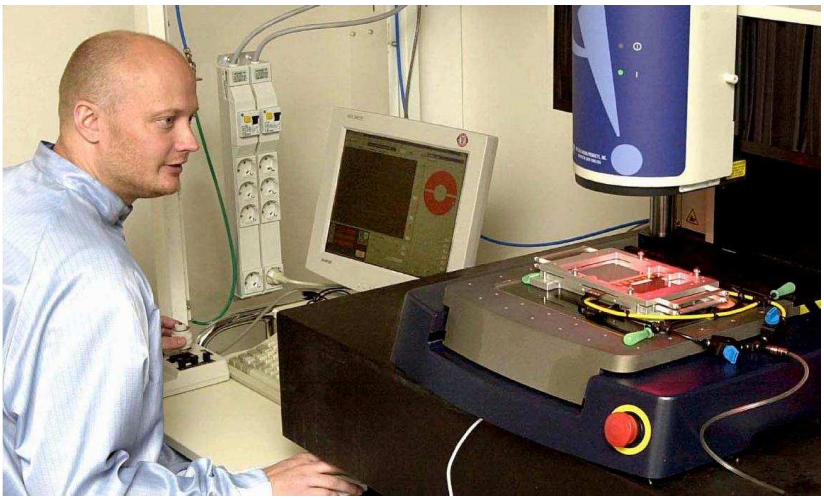

Figure 4: Module survey in progress.

[4]Optical Gaging Products, Inc., 850 Hudson Avenue, Rochester, New York 14621-4896, USA

The detector modules were surveyed three times during production. The first survey was performed immediately upon arrival in Uppsala. The second survey was performed after the hybrid had been mounted. The final survey was done after thermal cycling, long term test and final electrical tests and before the module was shipped to Oxford for mounting onto one of the SCT barrels. In the first survey the detector module was measured twice to crosscheck the validity of the results. The data from the first survey was reported back to Oslo, where it was used for tuning the assembly parameters. Unless the data in the second or final survey differed significantly from the results in the first survey, the measurement was done only once.

The XY-sequence measured the position fiducials located in the corners of each sensor, the position of the mounting hole and slot in the large facing of the module and two alignment circles on the hybrid. The sequence was run on both sides of the module, and the two measurement sets were coupled either through two pin-hole fiducials in the measurement jig or by measuring the corners of the upper side silicon plane. The 21 in-plane parameters were calculated from the measured raw data by an excel macro and resulta stored in excel spreadsheets. A measurement grid of 5 x 5 measurement points for each of the four detectors was used to calculate the out-of-plane parameters. The reference surface which was used to coupe the data from the two sides of the module was defined by the corner surfaces of the upper silicon surface. The reference plane for the survey of the upper side was defined by the upper surface of the corner while the reference plane for the lower side survey used the backside of the corner. To give both measurements the same reference plane, the lower side reference plane was corrected by the silicon thickness (285μm).

4 Electrical Testing

After hybrid bonding the completed modules were brought through extensive electrical testing. These tests set out to characterize the readout electronics[5], as well as ensure long term operational stability of the module.

The test setup is shown in figure 5. Six modules were tested in parallel, placed in an electrical and light shielded box, the "Test box" in the figure. The modules were mounted on an aluminium block, brought to the desired temperature by liquid cooling (alcohol) through pipes in the block. In order to maintain a low humidity, the box was constantly flushed with nitrogen.

For executing the electrical tests, a computer running the dedicated SCT test software SCTDAQ [5] under ROOT[6] was used, and the interfacing to the SCT modules were done through the VME modules SLOG and MuSTARD. Analog and digitial power to the module front end electronics were delivered and monitored by UppsDCS, developed in Uppsala and interfaced to SCTDAQ, while the detector bias voltage was delivered by a separate floating power supply, controlled and monitored from LabView.

SCTDAQ compromises a set of test macros, designed to test specific parts of the module. These are available as two sequences, the *Characterization sequence* and the *Confirmation sequence*, where the Confirmation sequence is a subset of the Characterization sequence. The test are summarized in table 1. In addition to the electrical tests, an IV scan is performed together with each sequence. See section 5 for more on IV scans.

[5] http://atlas.web.cern.ch/Atlas/GROUPS/INNER_DETECTOR/SCT/testdaq/testdaq.html

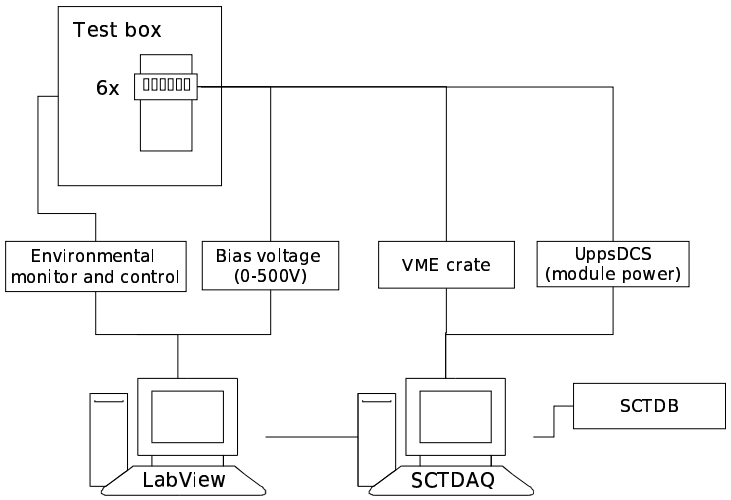

Figure 5: Schematic view of the electrical tests setup.

Test name	**Description**	**Conf**	**Char**
	Digital tests		
HardReset	Resets chips and checks that state after reset is as expected.	X	X
Redundancy test	Checks that both pairs of clock and command lines are operational.	X	X
Full bypass test	Tests alternative chip token routings on the hybrid.	X	X
Pipeline test	Tests the cells of the pipeline.		X
	Analog tests		
Strobe delay	Sets the correct timing for the calibration pulse.	X	X
Three point gain	Measures the gain, noise and discriminator offset of the analog circuitry by injecting three charges of 1.5, 2.0 and 2.5 fC.	X	X
Trim range	Attempts to bring all channels on a module into line with respect to the VT50 point (50% occupancy) at 1 fC injected charge.		X
Response curve	Same test as three point gain, but this time with 10 charges from 0.5 to 8.0 fC, to give a more thorough characterization of the readout circuitry with trimmed channels.		X
Noise occupancy	Measures # hits/# triggers at a 1 fC threshold with no input charge. This fraction translates directly to noise, and should be less than 5×10^{-4}.		X
Time walk	Measures the time stamp of a signal as a function of input charge. The variation with input charge should not be too large, $\sim$10 ns.		X

Table 1: Overview of electrical tests.

4.1 Test flow

Below is given an overview of the tests performed on a completed SCT barrel module. The tests were run at either 0 °C (cold) or 27 °C (warm) hybrid temperature. During all electrical tests the modules were biased at 200 V. After a completed test step, the data was published on web [6] and uploaded to the SCT DB[7], a common database for the whole SCT project.

- **PostBonding**. The first test run on the completed module, a warm characterisation sequence.
- **Thermal cycling**. An unpowered module is taken from +40°C to −20°C in 10 cycles. One cycle lasts for about one hour, to allow for temperature stabilisation.
- **Final metrology**. A final metrology is performed to ensure that the module is inside geometrical specifications after bonding and thermal cycling.
- **Long term test**. The module is powered, biased and triggered for 24 hours, and every second hour a confirmation sequence is run. Hybrid temperature is 0 °C.
- **Final characterisation**. Cold characterisation sequence.
- **Visual inspection**. A visual inspection of the module in order to ensure that the module show no physical irregularities.
- **PreShipment**. A final warm confirmation sequence is run before the module is shipped to Oxford for mounting on the SCT barrel.

4.2 Defective ASICs

Some ASICs that met all specifications at the level of wafer testing, developed a new set of defects during dicing and picking from wafers, which could not be spotted before mounted on hybrids. These defects where studied in detail at the Lawrence Berkeley National Laboratory [8] where 2/3 of the hybrids for the Scandinavian Cluster were produced. Whereas defects in the digital circuitry were considered fatal, it was found that decreased performance related to defects in the analog circuitry could be improved by adjusting the chip's front-end parameters. Given below is a short description of the most common problems related to defective ASICs, and how these problems were handled.

4.2.1 Block Low Gain

The ASICs with the Block Low Gain (BLG) defect have all a block of continous strips for which the gain is measured to be 10%–20% lower than the neighboring strips. As a consequence these channels receive a higher input noise since the input noise is calculated as the ratio between the output noise and the calculated gain. This higher input noise is the real problem for the BLG ASICs as they often fail our noise cut. See figure 6.

The BLG defect was discovered to be a timing problem [8], related to the fact that these channels with an effective lower gain have a higher gain at the preamplifier level.

[6] http://www4.tsl.uu.se/~Atlas/Electrical/ProductionMain.html
[7] http://wacap.unige.ch:3146/phyprdwww/sctprd/welcome.html

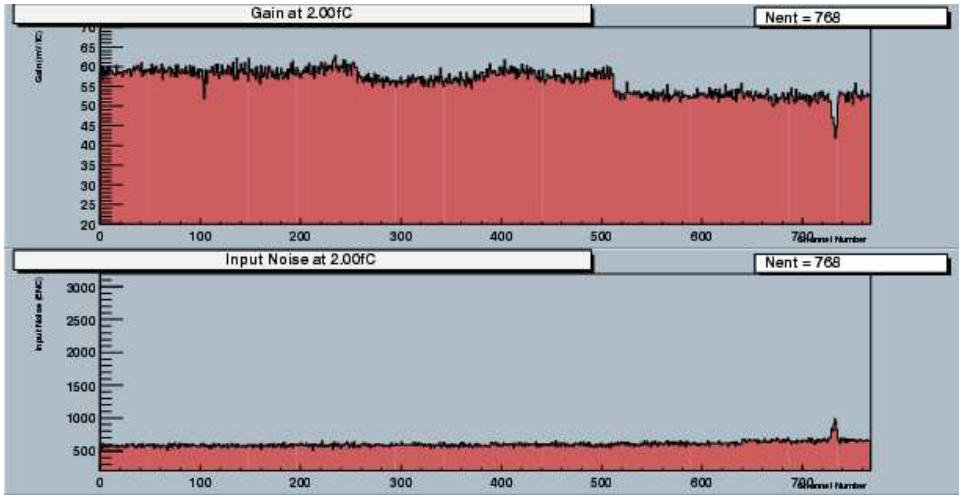

Figure 6: The dip in calculated gain seen at strip $\sim$ 735 for Scand module 192, results in an artificial excess input noise as seen in the lower plot.

The fast rise of the signal results in a shorter propagation delay, and since the strobe delay is calculated as a mean value for the entire chip the strobe delay is set to short for the BLG channels. Hence, increasing the strobe delay fraction from 0.25 to 0.40 (with respect to the leading edge) moves the strobe delay away from the leading edge of the BLG channels and increases their calculated gain. The excess noise for the BLG channels is consequently seen as an artifact of using too short strobe delay.

4.2.2 Large Gain Spread

Test results from wafer level show that some chips have a significantly different calculated gain when they are tested at the finished hybrid. The large difference suggests sensitivity to small changes in the operating conditions, and in [8] it was shown that Large Gain Spread (LGS) chips are more sensitive to changes in the shaper current (Ish) than good chips. At the nominal parameters (Ish = 30 μA and Vcc = 3.5V) the LGS chips have an average lower gain and also larger gain RMS than good chips. Lowering the shaper current Ish to 20μA increases the average gain of the LGS chips to an acceptable level, it also reduces the RMS value of the gain spread. Hence this made most LGS chips operate satisfactory.

4.2.3 8 fc effect

During ResponseCurve testing threshold scans are performed for several different input charges up to 8fc, and as previously explained gain, noise and offset are extracted from the function fitted to the response. Occasionally it was however seen that the 8fc scan gives larger response than to be expected from the extrapolation of the scans done with lower input charges. This effect is know as the "8fc effect" and is caused by a saturation of the threshold DAC. Hence discrimination of high pulses is impossible. The problem is solved by not taking the 8fc point into account when fitting the response curve if this effect is

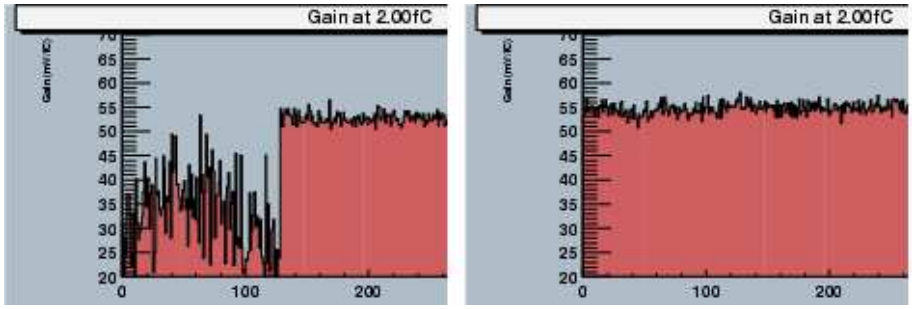

Figure 7: Scand module 136 showing a clear LGS effect on the left han side of the plot when running with nominal settings. Right hand side shows how the chip is recovered when the shaper current Ish is lowered to 20μA.

seen. During ATLAS data taking the SCT module will never operate at a 8fc threshold hence this has no practical influence.

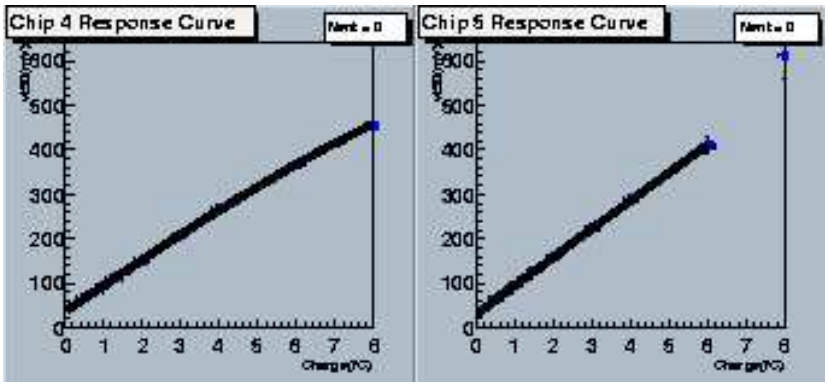

Figure 8: Chip E5 of Scand module 313 clearly shows a larger gain at the 8fc scan when compared to its neighbouring chips. The SCTDAQ software does not take this point into account when fitting the response curve.

4.2.4 S-curve oscillations

A significant number (see section 7) of the assembeled modules displayed coherant effect between channels seen as S-curve oscillations. An S-curve is a plot of efficiency vs threshold for a fixed input charge, see figure 9. A normal curve is supposed to show a smooth inverse S shape, as can be seen on the leftmost plot in figure 9. To the right a curve with oscillations is shown. The effect only appeared at low thresholds (0.0 - 0.5 fC) for low input charges (well below 1.0 fC). The oscillations was also usually more pronounced at the bottom side of a module (link1), increasing towards the end of the hybrid. No hybrids displayed the effect before module assembly. Relative to the other clusters, a higher ratio of assembled modules had this effect in the scandianvian cluster.
Considerable work was invested in order to find the source of this effect [7], and a summary of the investigation is presented here:

- **Temperature:** No correlation with module/environment temperature were found, the s-curves only showed minor changes with respect to temperature.
- **Grounding schemes:** The problem could be caused by non-optimal grounding schemes, so different grounding schemes where tested. This did not remove the effect, but the oscillations were found to be less prominent in particluarly noisy grounding schemes. This was expected, since the noise in these cases overshadows the oscillation effects.
- **Module gain:** Increasing the module gain revealed an increase also in the oscillations.
- **Module assembly:** Since hybrids did not show oscillations before module assembly, suspicion was that the effect was introduced by the assembly procedure used by the Scandinavian cluster. The assembly procedure was changed in order to minimize physical stress on the hybrid during gluing, but no effect due to this was seen. To try to further exclude this possibility, a scandinavian detector-baseboard sandwich together with a hybrid tested in Uppsala was sent to RAL for assembly, since RAL reported a very low rate of oscillating modules in their own production. The module displayed small to moderate oscillations, pointing in the direction of a module effect.
- **Test setup:** Testing a module at different test setups turned out to introduce variations in the s-curves. The various test locations used was Uppsala, Bergen, RAL, Cambridge and CERN. It was seen that some modules had very similar oscillations at all locations, while other modules showed considerably less oscillations at RAL and Cambridge sites.
- **Source test:** One module was tested with β-source to study iff top side had higher efficiency than bottom side. No difference was seen.

In the end, the oscillations were never fundamentally understood, but it was assumed not to have any effect on physics, since they only appear at low (0.0 - 0.5 fC) thresholds, while the SCT will run at a threshold of 1.0 fC. It was reported that similar effects was seen on hybrid prototypes during the design phase, and it was believed that the phenomenon was an effect due to components performing on the limit of required specifications. It is interesting to notice that the number of modules displaying this phenomenon decreased during the second half of the production, see section 7, without the scandinavian assembly/test setup being altered, again pointing in the direction of a module hardware effect.

4.2.5 Stuck Cell

Even though a mask register is provided for the ABCD3T chip this does not help in the case of a stuck cell. The mask register is situated in front of the pipeline and stuck cells in the pipeline will always be read out. This causes severe problems for the electrical testing since many parameter settings are set to the mean of the chip. The only way to solve this problem is to mask channels with stuck cells in SCTDAQ. Still channels with stuck cells are plotted in the Noise Occupancy scan, as seen from the S-curve on figure10. 4 modules produced by the Scand Cluster had channels with stuck cells, but none of them had more than 1 channel affected.

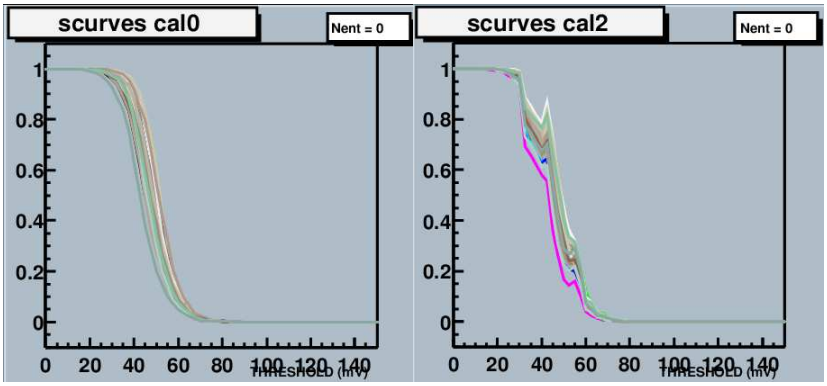

Figure 9: Example of normal (left) and oscillating (right) s-curves from module 006.

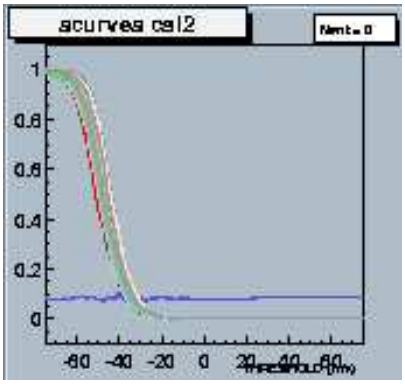

Figure 10: As the threshold is raised good channels produce less noise whereas channels with stuckcells are left on the same level. The reason for the 0.1 level shown here is related to the fact that the ABCD3T pipeline is a multiplexed 12*12 dynamic memory matrix and not a linear pipeline.

4.2.6 Other seen effects

Negative offset This effect was frequently seen for individual channels on the level of Hybrid testing, but with the increased noise level from the connected strips this problem cease to exist for most modules. Only one Scand module (module 190) had negative offset after bonding, but this does not imply any problems for the operation of this module.

5 IV testing

The IV characteristics of the silicon sensors were measured several times along the module assembly process. Acceptance tests of all silicon sensors used in the production was done by the manufacturer up to 350V and by the Bergen production site up to 500V. A single silicon sensor was accepted if the leakage current at 20°C was less than 6μA at 150V and less than 20μA at 350V. The IV characteristics had to be stable and repeatable[4].

Exclusively sensors that had passed the acceptance test were made into silicon detector

modules. After four sensors were glued into an assembly the IV-measurement up to 350V was repeated on individual sensors at the Oslo production site.

The completed silicon detector modules were tested directly after wire bonding to 110V. This test was introduced as a fast feed-back loop to allow tuning of the wire bonding parameters between modules. In electrical tests all silicon detector modules were tested in PostBonding sequence up to 500V. In the Final Characterisation sequence the modules that reached 500V without signs of breakdown in the PostBonding tests were retested to 500V. Modules with onset (a sudden rise in leakage current, see figure 11) before 500V were tested to 350V. In the PreShipment sequence all modules were tested to 350V to check that IV-characteristics remained unchanged. Modules that show breakdown below 500V have to pass a long term test showing that the current decays to normal leakage current value over a few hours. Figure 12 shows a characteristic decrease of leakage current for one detector module that has current onset around 440V. The bias voltage during the test was set to 500V.

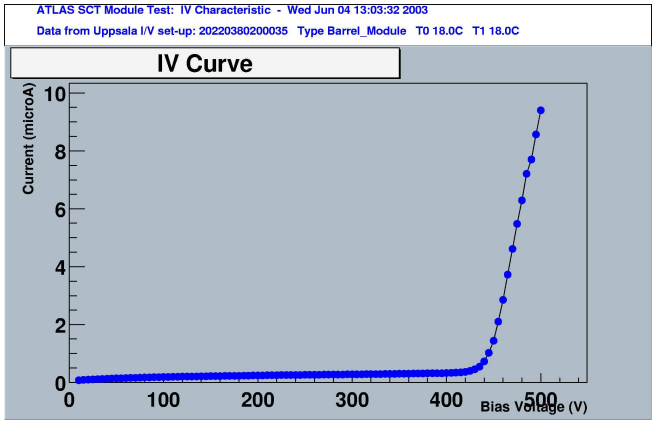

Figure 11: An IV-curve with onset at 440V.

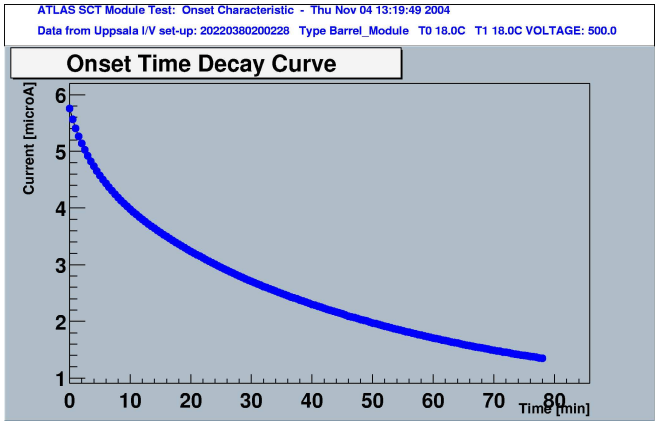

Figure 12: Decay of leakage current over time for a detector module.

5.1 Characteristics of unbonded detectors

A system to perform a variety of measurements on unbonded detectors was set up in Bergen in a clean-room environment. A description of the system can be found in [9]. A total of 1939 Hamamatsu detectors were tested. IV- and CV-scans as well as a visual inspection of the strip side and backside edges were performed.

The IV-scans were done from $0V - 500V$ with $10V$ steps and $10s$ settling time, applying the acceptance criteria described earlier. From the full set tested, 7 detectors were designated as B-quality: 6 of which had high currents at $500V$, although within requirements at $350V$, and one with high irregular current in the $1\mu A$-range from $30V - 500V$.

The remaining 1932 detectors were designated A-quality detectors, and had good IV-chracteristics. The current distribution of these detectors are seen in Figs. 13 — 15 with currents normalized to $20°C$. The high current tail of the plots have been excluded, but the maximum values are given for each plot.

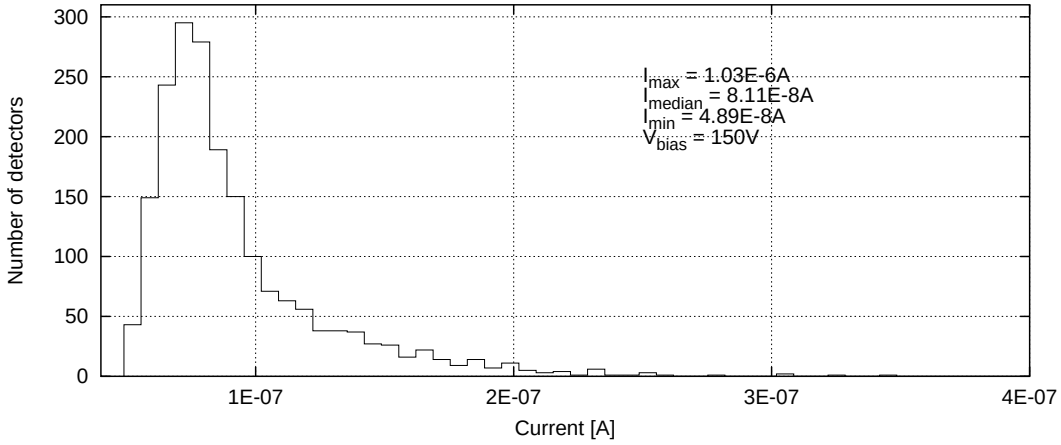

Figure 13: Current distribution at $150V$.

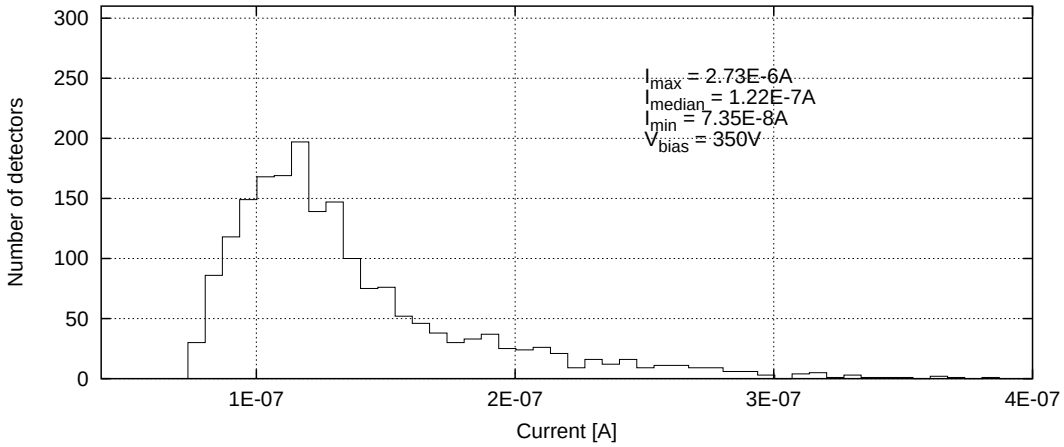

Figure 14: Current distribution at $350V$.

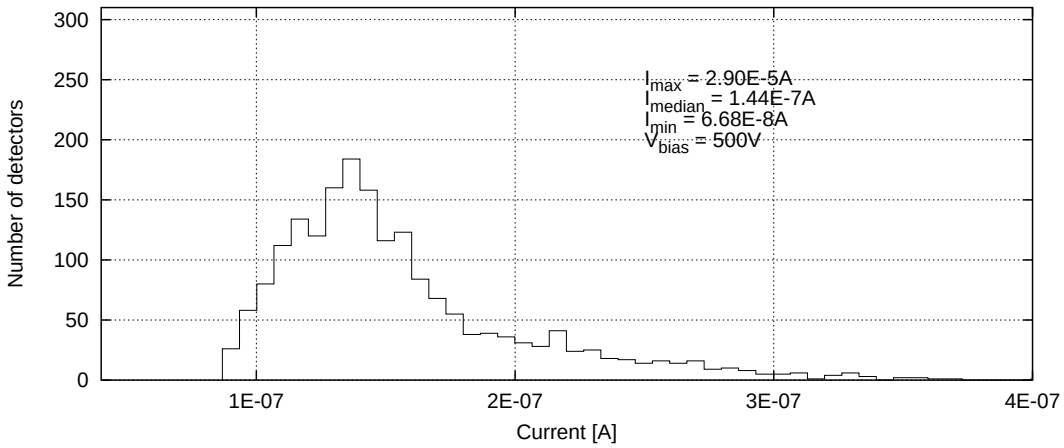

Figure 15: Current distribution at $500V$.

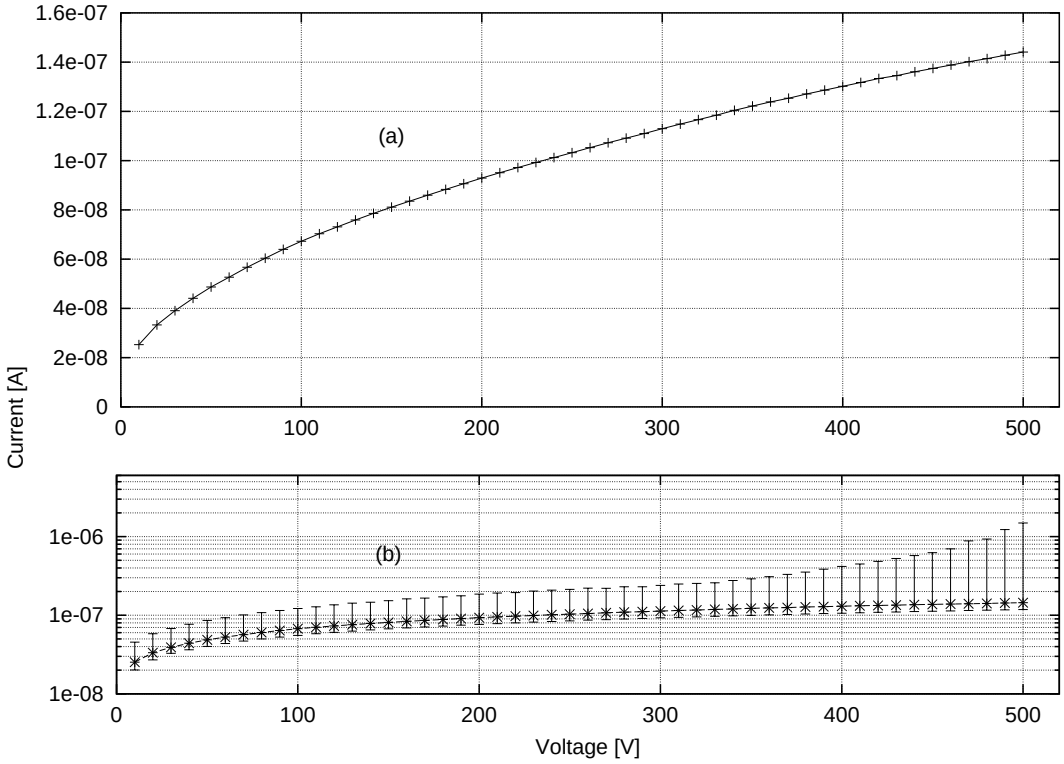

Figure 16: Current median values of 1932 Hamamatsu detectors from $10V$ to $500V$ **(a)**. The error bars included in **(b)** show the r.m.s. spread of the currents, calculated separately for detectors below and above the median.

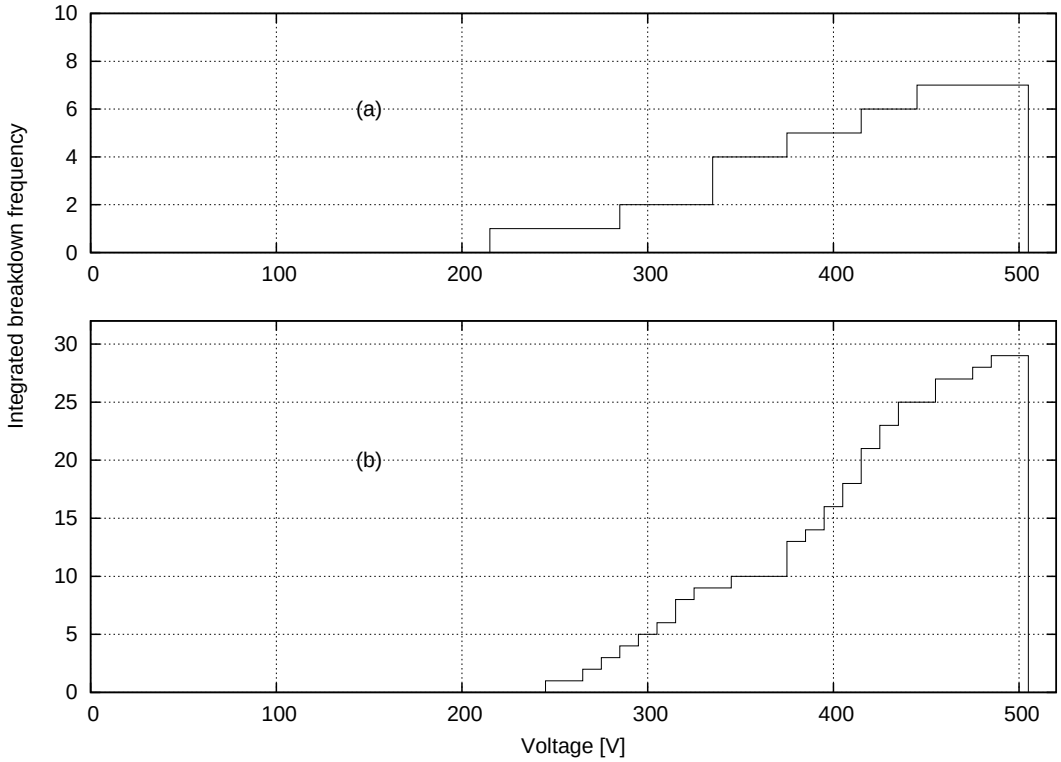

Figure 17: Integrated breakdown voltage thresholds for **(a)** detectors with $I_{max} \geq 20\mu A$ and **(b)** detectors with a distinct breakdown behaviour, but with $I_{max} < 20\mu A$.

The currents show an increasing spread for larger bias voltage, but with median values of $81.1nA$ and $122nA$ at $150V$ and $350V$ respectively that are appreciably well below the required limits. Fig. 16(a) shows the mean value of the 1932 detectors. Fig. 16(b) shows the same data with error bars that indicate an onset of breakdown for some detectors. The breakdown fraction of the 1932 detectors is very low, and is the reason why a median value representation has been chosen.

If breakdown behaviour is observed in a detector, the breakdown voltage threshold remains relatively stable when remeasured. Considering the full set of A- and B-quality detectors, Fig.17(a) shows the integrated distribution of breakdown voltage thresholds for detectors with $I_{max} \geq 20\mu A$. This corresponds to a breakdown fraction of 0.36%. These characteristics are considered critical only due to the high I_{max}, not the breakdown behaviour itself. Detectors with breakdown behaviour, but with $I_{max} < 20\mu A$, had an integrated breakdown voltage threshold as seen in Fig. 17(b). The maximum fraction of uncritical breakdowns at $500V$ is 1.50%, i.e. a total breakdown fraction of 1.86% for the full set. Avanlanche breakdown was not observed for any of the 1939 detectors.

5.1.1 Single strip defects

The detector manufacturer was required to supply single strip defect information for each detector. The five possible strip defects, as defined in Hamamatsu measurement files, were: *Pinhole*: Short through coupling oxide between *Al*-strip and implanted strip. *Short*: Short between two or more adjacent *Al*-strips, usually via excess *Al*; *Open*: A discontinuous *Al*-strip. *Implant short*: Short between two or more implanted strips. *Implant open*: Discontinuous implanted strip. According to requirements, no detector should have more than 2% defect strips, i.e. 15 strips. Additionally, each delivered batch should have at most 1% defect strips per detector on average.

Data from the full Hamamatsu set have been extracted and studied [9]. The defect types were, in decreasing order of domination: pinhole, *Al*-short, *Al* open and implant open. No detectors were reported to have shorted implants. Pinholes constituted $\sim 70\%$ of the defects. The maximum number of defect strips for a single detector is found to be 13 (only pinholes).

An average of 0.358 defect strips per detector was found, i.e. $\sim 0.05\%$ This is well within the requirements.

5.2 IV-characteristics of silicon detector modules

The silicon sensors produced by Hamamatsu were of good quality. The measured leakage current for the delivered sensors were well within the acceptance criteria. The typical leakage current for a sensors at 500V was below 0.25μA. Hence the sum of leakage current for four sensors in a perfect silicon detector module was below 1μA. Figure 18 shows the IV-characteristics for four individual sensors in a assembly and figure 19 shows the IV-curve for the completed module. Wire bonding impacts from time to time the IV-characteristic of the silicon detector module. The modules produced by the Scandinavian cluster were wire bonded in Uppsala with a Kulicke and Soffa wire bonding machine model 1470. The wedge used was Kulicke and Soffa 4WAVO-2025-W6C-MOO and wire 25 μm aluminum (Al/Si 1%). The wire bonding machine operates with 60 kHz ultrasonic frequency. The performance of the bonding machine was clearly on the limit to manage the difficult geometry of the module with large differences in heights between surfaces and the tight geometry. One parameter that in particular made the bonding process difficult to master was the glue pattern between the sensors and the TPG baseboard that didn't reach under the bonding pads which lead to insufficient support of the sensor during bonding. The variation in the support varied from module to module which made it difficult to find bonding parameters that would work for many modules. The most frequent bonding problem was no sticking bonds that had to be remade. The operation of removing incomplete bonds and rebonding the channel has a small probability of generating a defect. On rare occasions the wire slipped from the wedge and the wedge came in contact with the oxide surface on the sensor. A modern bonding machine with higher ultrasonic frequency, lower pressure would have reduced the power needed to make good bonds and reduced the defects created in the bonding process.

Detector modules with non perfect IV-curves [8] are all damaged in the bonding process. The defects are believed to be in the oxide layer or the silicon-oxide interface. The characteristics of the defects can be divided in three classes.

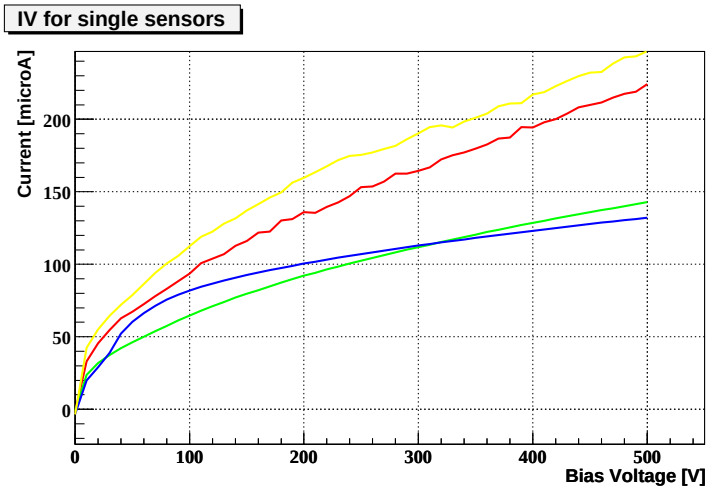

Figure 18: Leakage current characteristics for four silicon sensors glued in an assembly.

[8] The current of the detector module not equal the sum of current for the four sensors in the module.

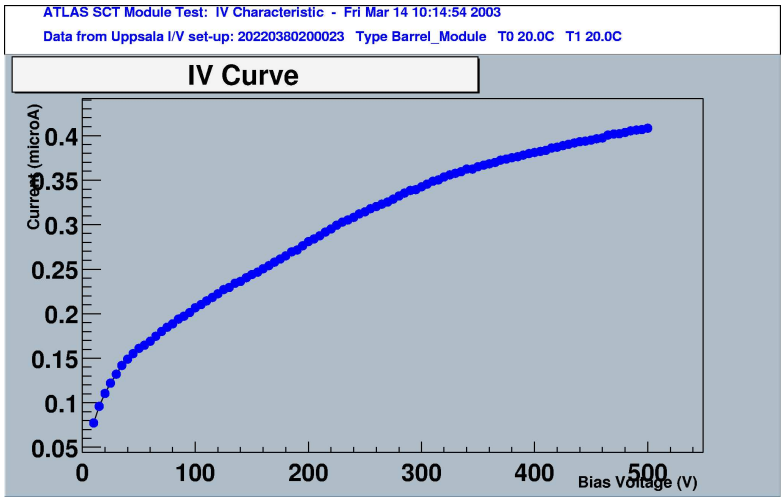

Figure 19: Leakage current characteristics for a completed module made with the sensors shown in figure 18.

- General current increase over the full voltage range from 0 v to 500 V, figure 20.
- Resistive behavior of the IV-curve, figure 21.
- Current onset at a voltage threshold, figure 11.

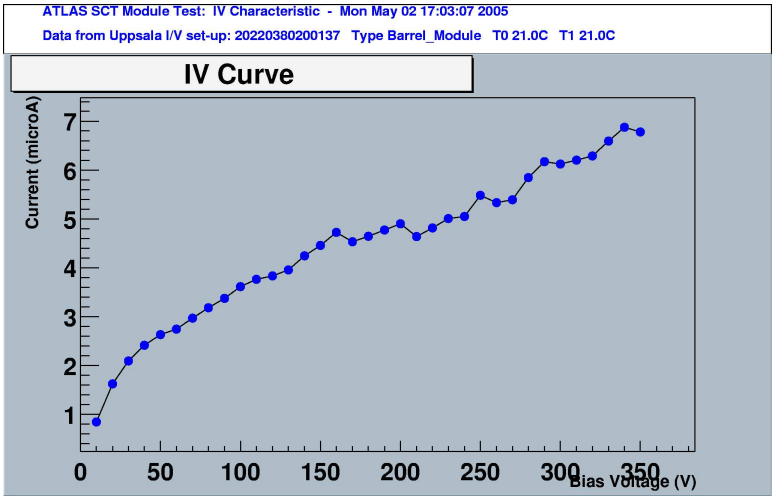

Figure 20: An IV-curve with a general current increase over the full voltage range.

The biggest yield loss of modules in the production was due to bad IV-characteristics. A module was accepted if the total leakage current at 500V at 20°C was below 4μA. Modules with current onset were accepted if the onset voltage was above 300V and the current long term test showed a decay of leakage current that is characteristic to detector

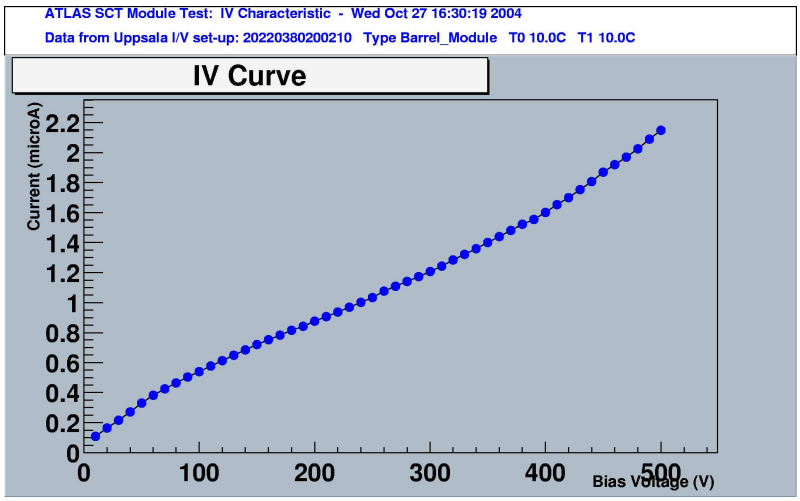

Figure 21: An IV-curve with a resistive rise.

modules with onset. Modules that didn't meet the acceptance criteria were not shipped to the Oxford assembly site.

6 Visual Inspection

Before shipment and before the last electrical test (PreShipment), all modules underwent thorough visual inspection. Using a microscope, the active detector surface was inspected as well as electronics and bonding wires. Any irregularities like gluemarks, grains of dust etc. were taken notice of, and comments with excact location were written in the Visual Inspection Report. The reports were uploaded to the SCT database for future reference. With the exception of shortcutted bondingwires and single strip defects, no correspondence was found between visual imperfections and the module's electrical performance.

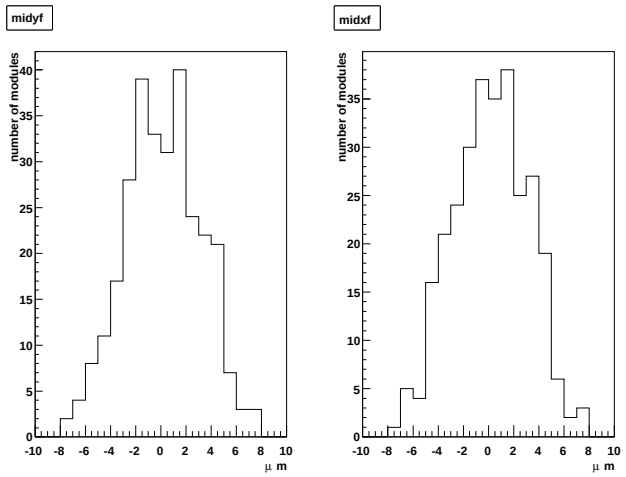

Figure 22: Transverse (left) and longitudinal (right) alignment parameter, midyf for 294 modules subjected to final metrology. Mean values and standard deviations are 0.23 (0.19) and 3.1 (2.9) μm respectively for midyf (midxf).

7 Production Results

Not counting 'site qualification' work, 318 Sensor-Baseboard (SB) assemblies were manufactured in Oslo. The number of detectors available for this production was 1282. About 15 of these were classified as 'use last', mostly because tendencies of micro-discharge were seen just below 350V while currents at 350V still were found to be well inside specification.

Of the 318 SB assemblies produced, 3 were rejected for further production because of misalignment during glueing, while 5 were rejected due to poor I-V characteristics after glueing. Of these, 3 were made with the 'use last' detectors, where poor IV performance was not a surprising result.

The total of 310 SB assemblies remaining matched well to the number of hybrids at our disposal: Of 316 hybrids received 4 were judged unsuitable for module prodction, leaving 312 to be potentially used. Here we report on the quality of these in addition to two site qualification modules, i.e. on the results for 314 modules.

7.1 Geometrical properties

SB Assemblies were mounted in Oslo, measured in Uppsala before hybrid mounting and bonding. After thermal cycling and electrical testing the geometric properties were found in a final series of measurements. It is these measurements that are used for module classification and in the figures presented here, for the 294 modules that were subjected to the final geometrical survey.

The tightest specification was on the back to front sensor alignment in the direction transverse to the strip direction summarized in a parameter named "midyf". The original specification for this was that the alignment should be better than 5 μm. As production progressed it was clear that a wider tolerance had to be accepted. However if measurements showed that the alignment was poorer than 15 μm the whole module was classified as a

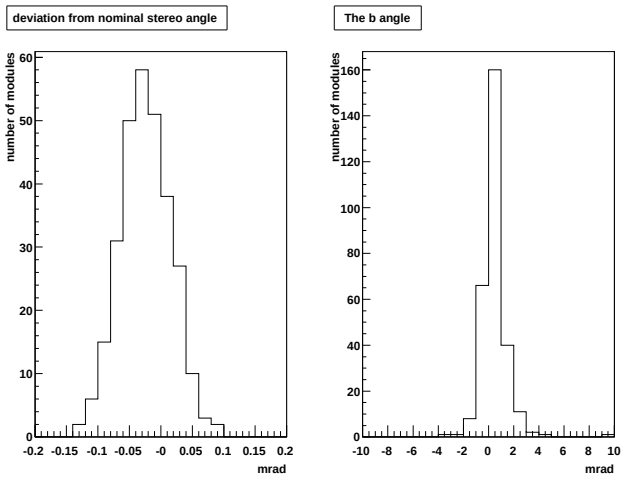

Figure 23: Deviation from nominal stereo (left) and b (right) angles for 294 modules subjected to final metrology. Means and standard deviations are -0.025 (0.46) and 0.04 (1.02) mrad respectively for the stereo (b) angles

'FAIL', and those between 10 and 15 μm were to be used as spares. Similar considerations were made for all the other geometry parameters.

In addition to the parameters connected to the XY alignment, out of plane geometry measurements were used to assess the quality of the glueing process, and to identify potential operating problems. Facings on each side of a module, which are used as mounting and contact points for module cooling, should lie in the same plane. The overall thickness of the module should not exceed the tolerances. Two modules were found to fail the geometrical tolerances after hybrid mounting, one had too large overall thickness, while the other one had a problem with the facings.

In the plots we show the measurements of some of the most critical geometrical parameters, midyf and midxf (fig. 22), the stereo and the b angles (fig. 23), and the two out of plane parameters describing the deviation of the detector shapes from the standard shape (fig. 24).

7.2 Electrical properties

Each module had to be subjected to 1536 detector to detector bonds, and to the same number of detector to hybrid bonds. This is a high risk process where the module can be easily damaged, in particular due to the pressure that has to be applied when placing the bonds. The result was that a number of modules failed due to unacceptably high leakage currents caused by the bonding process. The number of channels that did not receive a good bond could be kept well under control. Attempts to repair failing bonds were abandoned at an early stage because of a relatively high risk of damaging the module in some other way during repair work.

After bonding, the modules were subjected to a number of electrical tests, see section 4. The plots below summarize results from the Final Characterisation test. The number of bonding faults and the total number of bad channels are shown in fig. 25. The largest

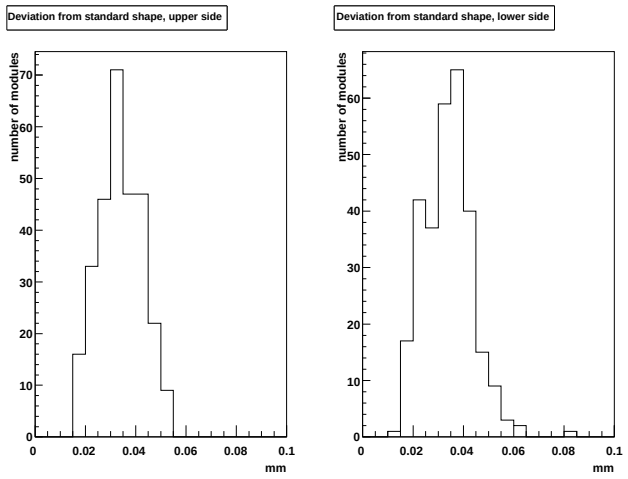

Figure 24: Out of plane deviations from standard shapes for the upper (lower) sides of the modules.

source of bad channels is due to bad channels in the ASICs. 79 (25 %) of the hybrids used in our production were found to have one or more defective channels in our initial testing. SCT policy was to group ASICS with one bad channel onto the same hybrid, so for a large number of the modules, a perfect assembly would still result in 12 bad channels.

Fig. 26 show the noise and noise occupancies measured for the modules. It is seen that noise occupancies are well within specification. The tail towards high noise occupancies consists of modules with 'stuck cell' channels. These are due to ASICs that are defect in such a way that one channel is always 'on', i.e. contributing to the noise occupancy all the time. See section 4.2.5.

The 'S-curve problem' was monitored throughout the production. Overall, 142 of 294 modules were found to have wiggly s-curves. However it was noted that modules mounted with hybrids received late in the poduction were much less likely to exhibit this feature. Dividing the production chronologically in two halves, the first half had a rate of 'problematic' curves of 66 % while the corresponding rate for the second half was just 31 %.

Figure 27 shows leakage currents at 350V and 500V extracted from the final IV scans. If breakdown effects were seen, the modules were not taken to 500V. The temperature at which these scans were done is not important for detecting breakdown effects, two settings for the temperature in different stages of the production, 18 and 14 degrees respectively.

7.3 Production Yield

A total of 288 modules were found to be useable for Atlas. This figure includes 20 modules deemed to be used as spares. The production yield out of 320 started modules is thus 90% (84%) including (excluding) spares. This yield estimate is slightly conservative in the sense that it includes the three SB assemblies started with 'use last' detectors. The target yield was 85% to allow for another 5% loss in the module mounting process, and it is seen that our figure is close to the target.

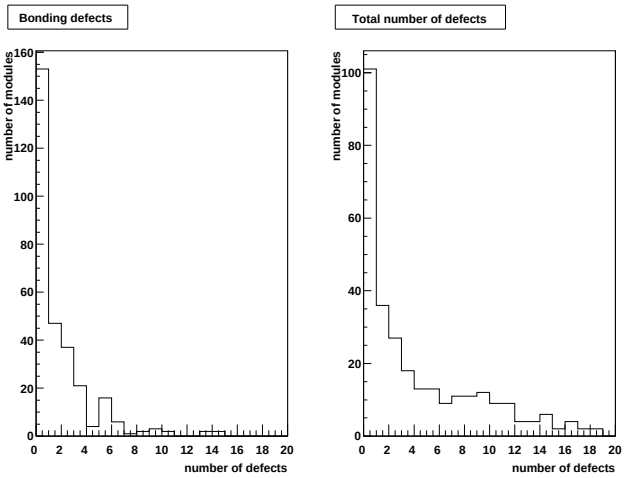

Figure 25: Number of bad bonds and total number of bad channels per module for 296 modules subjected to final electric characterisation. Means values are 1.49 and 4.01 channels respectively

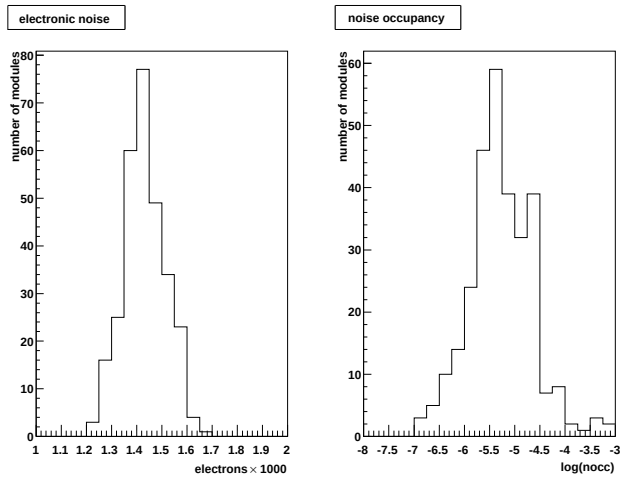

Figure 26: Electronic noise and $\log_{10}$ of the noise occupancy per channel at a threshold of 1 fC in 296 modules subjected to final electric characterisation. The mean of the noise plot is 1432 electrons with a standard deviaton of 86 electrons. Means, median and standard deviation of the noise occupancy are $2.1 \times 10^{-5}, 4.9 \times 10^{-6}$ and 7.3×10^{-5} respectively.

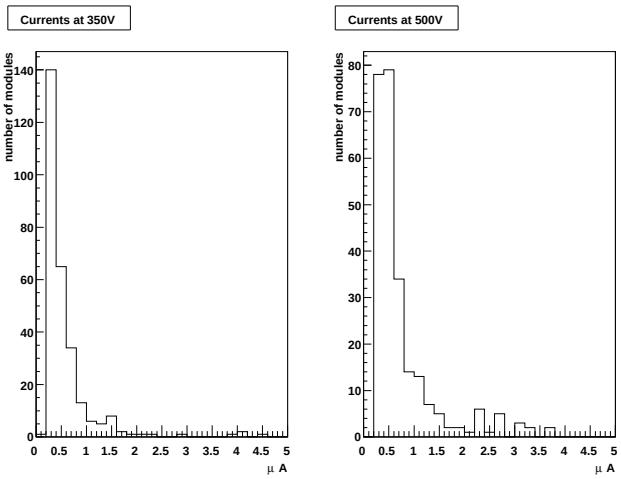

Figure 27: Leakage currents for modules subjected to final IV scans to 350V (left) and 500V (right), in μA. Mean median and standard deviations are 1.00 (1.56), 0.41 (0.53) and 2.63 (3.48) μA respectively at 350 (500) V.

8 Conclusion

A distributed production line has been set up in Scandinavia for manufacturing silicon detector modules for the Barrel SCT. The Scandinavian Cluster with participating institutes from Bergen, Oslo in Norway and Uppsala in Sweden has successfully delivered more than 270 modules to for the Barrel SCT. The modules delivered fully satisfy the specifications, as described in this note. The delivery is the result of a major effort over many years of the three groups involved. We wish to thank our colleagues of Barrel SCT as well as the whole SCT community for very constructive collaboration. Thanks also to our home institutes and to the funding agencies of Norway and Sweden.

References

[1] ATLAS Inner Detector Community
ATLAS Inner Detector TDR,
ATLAS TDR 4, CERN/LHCC/97-16, ISBN 92-9083-102-2, 30 April 1997

[2] S. Snow and A. Weidberg
The effect of inner detector misalignment on track resolution,
ATL-INDET-97-160, March 3, 1997.

[3] ATLAS Barrel Module Community
ATLAS SCT Barrel Module FDR/2001,
SCT-BM-FDR-7 July 11, 2001.

[4] ATLAS Barrel Module Community
Appendix to SCT-BM-FDR-5.1/2001,

Detector Technical Specification, Extracted from the 1999 Tender and Contract Documents, using the example of CERN being the Contract partner.

[5] F. Campabadal, C. Fleta, M. Key, M. Lozano, C. Martinez, G. Pellegrini, J.M. Rafi, M. Ullan, L.G. Johansen, B. Mohn et al.
Design and performance of the ABCD3TA ASIC for readout of silicon strip detectors in the ATLAS semiconductor tracker,
Nucl. Instrum. Methods Phys. Res., Sect A 552, (2005), 3, 292-328

[6] Rene Brun and Fons Rademakers,
ROOT - An Object Oriented Data Analysis Framework,
Proceedings AIHENP'96 Workshop, Lausanne, Sep. 1996,
Nucl. Inst. & Meth. in Phys. Res. A 389 (1997) 81-86.

[7] Ola Kristoffer Øye
A setup for electrical tests of ATLAS SCT barrel modules.
Cand. scient thesis, University of Bergen, April 2003.

[8] Alessandra Ciocio
Diagnostic Tools for Silicon Strips
Detector Readout during Module Production.
Presentation at the 5th Symposium On the Development And Application of Semoconductor Tracking Detectors, Hiroshima, Japan, 2004.
Nucl. Instrum. Methods Phys. Res., Sect A 538, (2005), 384-407

[9] Lars Gimmestad Johansen
Radiation hard silicon microstrip detectors in ATLAS at CERN.
Dr. scient thesis, University of Bergen, ISBN 82-308-0032-4, 2005.